

Multi Task Denoiser Training for Solving Linear Inverse Problems

Clément Bled*
cbled@tcd.ie
Trinity College
Dublin, Ireland

François Pitié
frcs@tcd.ie
Trinity College
Dublin, Ireland

Abstract

Plug-and-Play Priors (PnP) and Regularisation by Denoising (RED) have established that image denoisers can effectively replace traditional regularisers in linear inverse problem solvers for tasks like super-resolution, demosaicing, and inpainting. It is now well established in the literature that a denoiser’s residual links to the gradient of the image log prior (Miyasawa and Tweedie), enabling iterative, gradient ascent-based image generation (e.g., diffusion models), as well as new methods for solving inverse problems. Building on this, we propose enhancing Kadkhodaie and Simoncelli’s gradient-based inverse solvers by fine-tuning the denoiser within the iterative solving process itself. Training the denoiser end-to-end across the solver framework and simultaneously across multiple tasks yields a single, versatile denoiser optimised for inverse problems. We demonstrate that even a simple baseline model fine-tuned this way achieves an average PSNR improvement of +1.34 dB across six diverse inverse problems while reducing the required iterations. Furthermore, we analyse the fine-tuned denoiser’s properties, finding that its optimisation objective implicitly shifts from minimising standard denoising error (MMSE) towards approximating an ideal prior gradient specifically tailored for guiding inverse recovery.

CCS Concepts

• **Computing methodologies** → **Reconstruction**; *Learning from implicit feedback*; *Neural networks*.

Keywords

Linear Inverse Problems, Plug and Play Priors, Deep Learning, Diffusion, Denoising, Inpainting, Super Resolution,

ACM Reference Format:

Clément Bled and François Pitié. 2025. Multi Task Denoiser Training for Solving Linear Inverse Problems. In *European Conference on Visual Media Production (CVMP ’25)*, December 3–4, 2025, London, United Kingdom. ACM, New York, NY, USA, 9 pages. <https://doi.org/10.1145/3756863.3769703>

1 Introduction

Denoising networks [Bled and Pitié 2022; Guo et al. 2019; Liang et al. 2024; Liu et al. 2021; Qiao et al. 2017; Ren et al. 2022; Tassano et al. 2019, 2020; Yan et al. 2020; Yue et al. 2023; Zhang et al. 2017a] have achieved remarkable success by implicitly learning intricate image priors from massive datasets. These networks excel at removing

noise while preserving fine details and structural information, suggesting that they have captured fundamental properties of natural images.

Leveraging this implicit knowledge, recent research has explored using denoisers as priors for solving inverse problems. This prior was first indirectly exposed through the “Plug-and-Play” priors (PnP) approach by Venkatakrishnan [Venkatakrishnan et al. 2013] by incorporating denoisers into the regularisation term of the optimisation problem. More recently, Kadkhodaie and Simoncelli [Kadkhodaie and Simoncelli 2021, 2020] were able to make a direct connection between the denoiser and the prior $p(x)$ by exploiting Tweedie [Robbins 1992] and Miyasawa’s [Miyasawa et al. 1961] relationship between the residual image of a blind AWGN denoiser, $\hat{x}(y) - y$ and the gradient of the log-likelihood of the image:

$$\hat{x}(y) - y = \frac{1}{\sigma^2} \nabla_y \log p(y), \quad (1)$$

Although this connection was not explicitly made at the time, it also underpins the functionality of contemporary diffusion models [Dhariwal and Nichol 2021; Lu et al. 2024; Nichol and Dhariwal 2021; Sohl-Dickstein et al. 2015; Song et al. 2020; Tan et al. 2024; Wu et al. 2024a,b]. While both PnP methods and Kadkhodaie’s solvers present iterative approaches for solving linear inverse problems, the former relies on using denoisers as a regulariser within an optimisation framework, whereas the latter leverages Equation 1, offering a more streamlined approach.

In this paper, we propose to take this problem on its head and demonstrate that the implicit image prior captured by the denoiser can be fine-tuned through Kadkhodaie’s framework to improve its versatility as a problem-solving network. To accomplish this, we embed a pre-trained denoiser within the iterative framework and fine-tune it to generalise more effectively across tasks such as image super-resolution, inpainting, and demosaicing. By retraining the denoiser, we once again transform the natural denoiser prior into a universal image solver capable of addressing a wide array of imaging challenges. Our key contributions are thus as follows.

- We demonstrate the effectiveness of fine-tuning a denoiser within the framework of Kadkhodaie and Simoncelli for improved linear inverse problem solving.
- We evaluate the performance of the fine-tuned denoiser for use on various inverse problems, including super-resolution, inpainting, and demosaicing
- We analyse the impact of fine-tuning on the denoiser’s general denoising performance.

CVMP ’25, London, United Kingdom

© 2025 ACM.

This is the author’s version of the work. It is posted here for your personal use. Not for redistribution. The definitive Version of Record was published in *European Conference on Visual Media Production (CVMP ’25)*, December 3–4, 2025, London, United Kingdom, <https://doi.org/10.1145/3756863.3769703>.

2 Background

2.1 Plug-and-Play Prior

The concept of using non-deep-learning denoisers to tackle a variety of imaging problems was first introduced in 2013 by Venkatakrishnan, Bouman, and Wohlberg [Venkatakrishnan et al. 2013] in their *Plug-and-Play Prior* (PnP) framework. By treating these sophisticated denoisers as priors within an optimisation setup, they demonstrated how existing denoising algorithms could be repurposed to solve inverse problems. In classical inverse problems, the objective is to estimate the unknown image \hat{x} by solving:

$$\hat{x} = \arg \min_x \{l(y; x) + \beta s(x)\},$$

where $l(y; x)$ represents the data-fidelity term, $s(x)$ is a regulariser encoding prior knowledge of natural images and β controls the weight of the prior. Plug-and-Play (PnP) methods use variable splitting to separate data-fidelity from prior terms. Instead of directly minimizing both together, they introduce an auxiliary slack variable, traditionally updated via the Alternating Direction Method of Multipliers (ADMM) [Boyd et al. 2011]. In PnP, the denoiser acts as a proxy for this slack variable, serving as an implicit prior that guides the solution without requiring an explicit analytic prior function.

This innovation demonstrated the potential of state-of-the-art denoisers for inverse problems such as X-ray, MRI [Venkatakrishnan et al. 2013] reconstruction and super-resolution [Brifman et al. 2016]. This framework has since then been simplified [Romano et al. 2017] and extended to DNN denoisers [Zhang et al. 2021, 2017b]. These advances demonstrated significant improvements across tasks like deblurring, super-resolution, and demosaicing, solidifying PnP’s versatility.

2.2 Solving Inverse Problems Using Denoisers Implicit Priors

In contrast to PnP’s indirect approach, Kadkhodaie and Simoncelli introduced a new method that allows the denoiser image prior to be used more directly, enhancing the interpretability and effectiveness of inverse problem solutions. This method relies on the rediscovered Tweedie-Miyasawa [Efron 2011; Miyasawa et al. 1961; Robbins 1992] result, expressed in Equation 1, which provides a mathematical connection between the denoising residual and the gradient of the log-probability. While this interpretation is mathematically equivalent to that used in diffusion models [Daras et al. 2024], we continue with Kadkhodaie’s formulation for its simplicity and clarity in illustrating the iterative solving framework.

Leveraging this result, Kadkhodaie and Simoncelli created a framework to approach the low-dimensional manifold of real images, which maximises $p(x)$, within the high-dimensional space of possible images \mathbb{R}^N (with N the number of pixels). Their method generates an image x by starting with random noise y_0 and iteratively taking steps along the gradient of the log prior by applying a denoiser. This approach allows the synthesis of realistic images that lie on the high-probability manifold of natural images.

The method can be extended to solve inverse linear problems by placing linear constraints on a noisy image through a low-rank measurement matrix $x^c = M^T x$, where x^c is the vector of measurements. For example, in super-resolution, M^T represents a downsampling

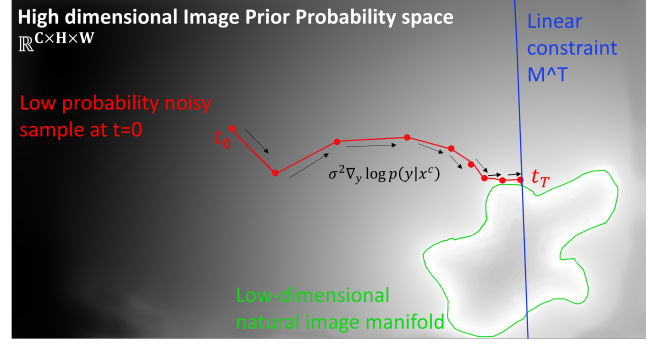


Figure 1: Illustration of solving a linear inverse problem in image probability space $\mathbb{R}^{C \times H \times W}$. Starting from a low-probability sample y_0 (red point, left), the solution is iteratively refined via gradient ascent on the log posterior $\nabla_y \log p(y | x^c)$, guided by the denoiser’s residual. The red trajectory represents the evolution of the sample toward higher-probability regions, constrained to remain within the linear subspace defined by the data fidelity constraint $M^T y = x^c$ (blue line). The solution converges near the natural image manifold (outlined in green), which captures high-probability images under the learned prior.

Algorithm 1 Universal Inverse Solver as defined in [Kadkhodaie and Simoncelli 2020]

```

1: Parameters:  $\sigma_0, \sigma_L, h_0, \beta, M, x^c$ 
2: Initialization:  $t \leftarrow 1$ ;
3: Draw  $y_0 \sim \mathcal{N}(0.5(I - MM^T)e + Mx^c, \sigma_0^2 I)$ , with  $e = [1, \dots, 1]^T$ 
4: while  $\sigma_{t-1} \leq \sigma_L$  do
5:    $h_t \leftarrow \frac{h_0 t}{1 + h_0(t-1)}$ 
6:    $d_t \leftarrow (I - MM^T)(\hat{x}_{t-1} - y_{t-1}) + M(x^c - M^T y_{t-1})$ 
7:    $\gamma_t^2 \leftarrow ((1 - \beta h_t)^2 - (1 - h_t)^2) \frac{\|d_t\|^2}{N}$ 
8:    $y_t \leftarrow y_{t-1} + h_t d_t + \gamma_t z_t$  with  $z_t \sim \mathcal{N}(0, I)$ 
9:    $t \leftarrow t + 1$ 
10: end while

```

operation. Without loss of generality, Kadkhodaie and Simoncelli assume that M and M^T are semi-orthogonal, which implies that M is the pseudo-inverse of M^T and that MM^T can be used to project an image onto the measurement subspace. With these constraints, the gradient of the conditional density can be derived as:

$$\sigma^2 \nabla_y \log p(y | x^c) = (I - MM^T)(\hat{x} - y) + M(x^c - M^T y), \quad (2)$$

where I is the identity matrix. This conditional gradient can then be used within a gradient-ascent iterative scheme:

$$y_t \leftarrow y_{t-1} + h_t \sigma^2 \nabla_y \log p(y | x^c) + \gamma_t z_t, \quad (3)$$

where, at iteration t , the step size for the gradient is controlled by h_t and the amount of noise $z_t \sim \mathcal{N}(0, \sigma^2 = 1)$ is controlled by γ_t . Scheduling for h_t and γ_t is parametrised by hyper-parameters σ_0, σ_L, h_0 and β (see original paper). For convenience, the overall algorithm is reported in Algorithm 1.

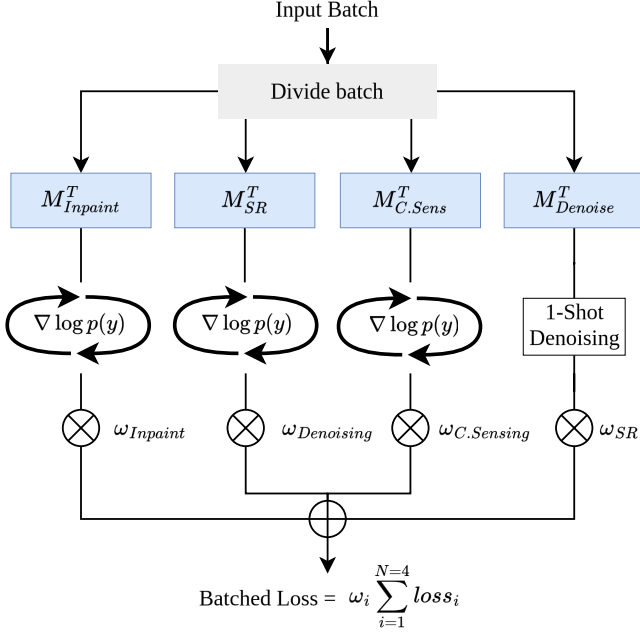


Figure 2: Illustration of our multi-task training framework. An input batch is divided into subsets for each inverse problem (inpainting, super-resolution, compressed sensing, and denoising). Each subset is passed through a task-specific forward operator M^T to produce the measurement vectors x_i^c , then, output images are iteratively reconstructed using a shared denoiser model that produces gradient estimates $\nabla \log p(y)$. The circular arrows represent the iterative refinement process. Each task output is used to compute a reconstruction loss, weighted by task-specific coefficients ω_i , and summed to form the final training loss.

3 Fine-Tuning Denoisers For Solving Inverse Problems

Kadkhodaie and Simoncelli’s method hinges on using a pre-trained blind denoiser to approximate the log prior’s gradient within their iterative solver. A key strength of this method is its adaptability, enabling the use of any compatible denoiser across various inverse problems. Recognising that the denoiser’s characteristics will significantly affect the iterative method’s outcome, a crucial question arises: can the denoiser be specifically optimised to enhance performance when applied in this manner to solve inverse problems?

3.1 Differentiable Training Platform for the Denoiser

To this end, we introduce a multi-task training platform designed to fine-tune a denoiser by integrating it directly into the iterative solver and training it on multiple linear inverse problem tasks (see Figure 2). A key aspect of our approach is treating the complete reconstruction as a differentiable computation graph. In training, a degraded input is fed through multiple iterations of the solver, with each step utilising the denoiser, until the final reconstruction is achieved. An image quality loss (L_1) is calculated on this final

output and propagated backward through all intermediate stages to update the denoiser’s parameters. Consequently, the network learns from a diverse distribution of intermediate reconstructions, enhancing its ability to generalize to the data encountered during iterative inverse problem solving.

3.2 Fixing the Number of Iterations

To enable training, we need to modify the original framework. In the original formulation, iterations proceed until the solution is deemed sufficiently smooth, specifically, when the standard deviation of the image residual falls below a predefined threshold. While appropriate for inference, this convergence-based stopping criterion is impractical for training, as it requires hundreds or thousands of iterations and results in inconsistent iteration counts across different images in the batch. To address this, we remove the smoothness-based termination condition and instead fix the number of iterations per training step. This not only standardises the training loop, but also enables backpropagation through a consistent unrolled graph. The selection of an appropriate iteration count and associated hyperparameters is addressed in Section 4.4.

3.3 Generalising the Denoiser via Multi-Task Training

To promote generalisation, we aim to fine-tune the denoiser not for a single inverse problem, but for a broader class of linear degradation processes. Rather than optimising it on a fixed task or constraint, we expose the denoiser to a variety of forward models during training. By applying the same network across different iterative reconstruction pipelines, the denoiser learns to produce gradient estimates that remain effective across a range of input conditions. This approach encourages the model to internalise a more flexible and broadly applicable image prior, rather than one tailored to a single inverse mapping. The specific set of tasks and their configuration are detailed in Section 5.1.

Figure 2 presents a generalised illustration of this training process. For each training step, a batch of B images is divided across N tasks. Each mini-batch is assigned a task and processed using a corresponding task-specific measurement operator M_{task}^T . The same denoiser is then applied iteratively within each task’s reconstruction pipeline to solve the constrained gradient ascent problem. This produces N task-specific losses, which are scaled by corresponding weighting factors (see Section 5.2) and summed to produce the overall training loss used to update the denoiser parameters.

4 Experimental Setup

With the training framework outlined, we now need to establish the training and test datasets, the deep learning architecture used for fine-tuning during experimentation, as well as the hyperparameters that were tuned according to the fixed number of iterations.

4.1 Inverse Problem Tasks

In our experiments, we include the tasks from the original paper, where the semi-orthogonal measurement matrices M_{task}^T project the image x onto a lower-dimensional subspace x^c . We additionally introduce demosaicing as a new task.

Super-Resolution. M^T is a downsampling matrix represented as a convolution kernel K , where the convolution has stride 2 and kernel averages pixels over non-overlapping regions $K = \frac{1}{4} \begin{bmatrix} 1 & 1 \\ 1 & 1 \end{bmatrix}$.

Inpainting. The measurement matrix M^T is a binary diagonal mask matrix, where the elements on the diagonal are set to zero or one, depending on whether that pixel falls within the missing region or not. In this task, the missing region is set to be 16×16 block, randomly positioned.

Compressive Sensing. This task [Donoho 2006] aims to recover signals from a small number of random linear measurements. In this scenario, we will consider that only 10% of the pixels are randomly preserved. This M^T matrix is defined in a similar way to the inpainting case.

Demosaicing. For demosaicing, M^T follows the Bayer Colour Filter Array (CFA) pattern, where each 2×2 block contains one red, two green, and one blue pixel. The diagonal entries of M^T are, again, binary values indicating the availability of the colour channels.

Frequency Super-Resolution. In this process, the 2D FFT of x is computed, and a mask W is applied to zero out a fraction of the high-frequency coefficients (e.g., 20%). Following the masking step, an inverse FFT is performed to obtain a low-resolution spatial-domain approximation: $x^c = \text{IFFT}(W \cdot \text{FFT}(x))$, where $\text{FFT}(x)$ and IFFT represent the Fourier transform and its inverse, respectively.

Random Basis Projection. For random basis projection, M^T maps the image vector $x \in \mathbb{R}^{HW}$ onto a lower-dimensional subspace using a random semi-orthogonal measurement matrix $M^T \in \mathbb{R}^{HW \times K}$, where $K = HW/5$.

4.2 Training/Testing Set

The training dataset consists of 3,400 uncropped images selected from DIV2K [Agustsson and Timofte 2017] and LSDIR [Li et al. 2023].

Our test set for all of our experiments will be the 100 images from the BSD100 [Martin et al. 2001] dataset.

4.3 Choice of Baseline Denoiser

Our choice of baseline denoiser follows, as in Kadkhodaie and Simoncelli [Kadkhodaie and Simoncelli 2020], a BF-CNN architecture. This is essentially a modification of DnCNN [Mohan et al. 2019] that removes biases from convolutional and batch normalisation layers, enabling improved generalisation across a wide range of input noise levels.

4.4 Hyperparameter Tuning for Fixed Number of Iterations

To reduce the number of iterations, the smoothness criterion is replaced with a fixed iteration count based on task difficulty. By constraining the algorithm to a set number of iterations, hyperparameters must be adjusted to ensure convergence within this limit. The key hyperparameters are β , which controls reintroduced noise; h_0 , the initial step size; and σ_0 , the starting noise level. For most tasks, starting with a heavily noised version of the constrained image (e.g., $\sigma_0 = 0.8$) is sufficient to achieve smooth results, avoiding

Table 1: Hyperparameters for Short and Long task configurations. The number of iterations per task is fixed to enable batched training, with other parameters (β , h_0 , and σ_0) adjusted to ensure convergence.

Configuration	Iterations	β	h_0	σ_0
Short	25	0.4	0.10	0.6
Medium	50	0.2	0.09	0.8
Long	100	0.06	0.5	0.08

the need for the higher noise levels ($\sigma_0 = 1$) typically used in the original framework.

We observed that different tasks converge at varying rates, which motivated the creation of separate iteration configurations: *short*, *medium*, and *long*. Super-resolution and frequency super-resolution are assigned the *short* configuration, while inpainting, compressed sensing, demosaicing, and random basis reconstruction are assigned the *medium* configuration, as summarised in Table 1. Additionally, a *long* configuration is introduced to evaluate the potential benefits of allowing the solver to run for an extended number of iterations for all tasks.

4.5 Training Details

During training, input images are cropped to 96×96 and augmented with random flips and rotations. Each task is supervised using the mean squared error (MSE) loss, and optimisation is performed with the AdamW optimiser over 500 epochs. A cosine annealing learning rate scheduler with warm restarts is employed: the learning rate is initially decreased from 10^{-3} to zero over the first 100 epochs, then reset and decayed to zero every subsequent 50 epochs. To accommodate the high memory demands of unrolled backpropagation through the iterative solver, the batch size is limited to 16.

5 Experiments

In this section, we present a series of experiments designed to evaluate the feasibility and effectiveness of fine-tuning a denoiser within an iterative framework for linear inverse problems. We begin by assessing whether fine-tuning improves task performance compared to a fixed, pre-trained model. We then investigate the denoiser’s ability to generalise to unseen tasks when trained jointly on multiple inverse problems. To address the challenge of balancing task-specific objectives during multi-task training, we explore various loss weighting strategies. Finally, we examine how fixing the number of iterations, rather than relying on convergence, impacts the quality and efficiency of the resulting reconstructions.

5.1 Multi-Task Training Scenarios

We conduct a series of fine-tuning experiments to assess how well a denoiser can generalise across multiple inverse problems when trained with multiple objectives. Three tasks, frequency super-resolution, random basis reconstruction, and demosaicing, are excluded from training and instead used as benchmarks to evaluate generalisation to unseen problems.

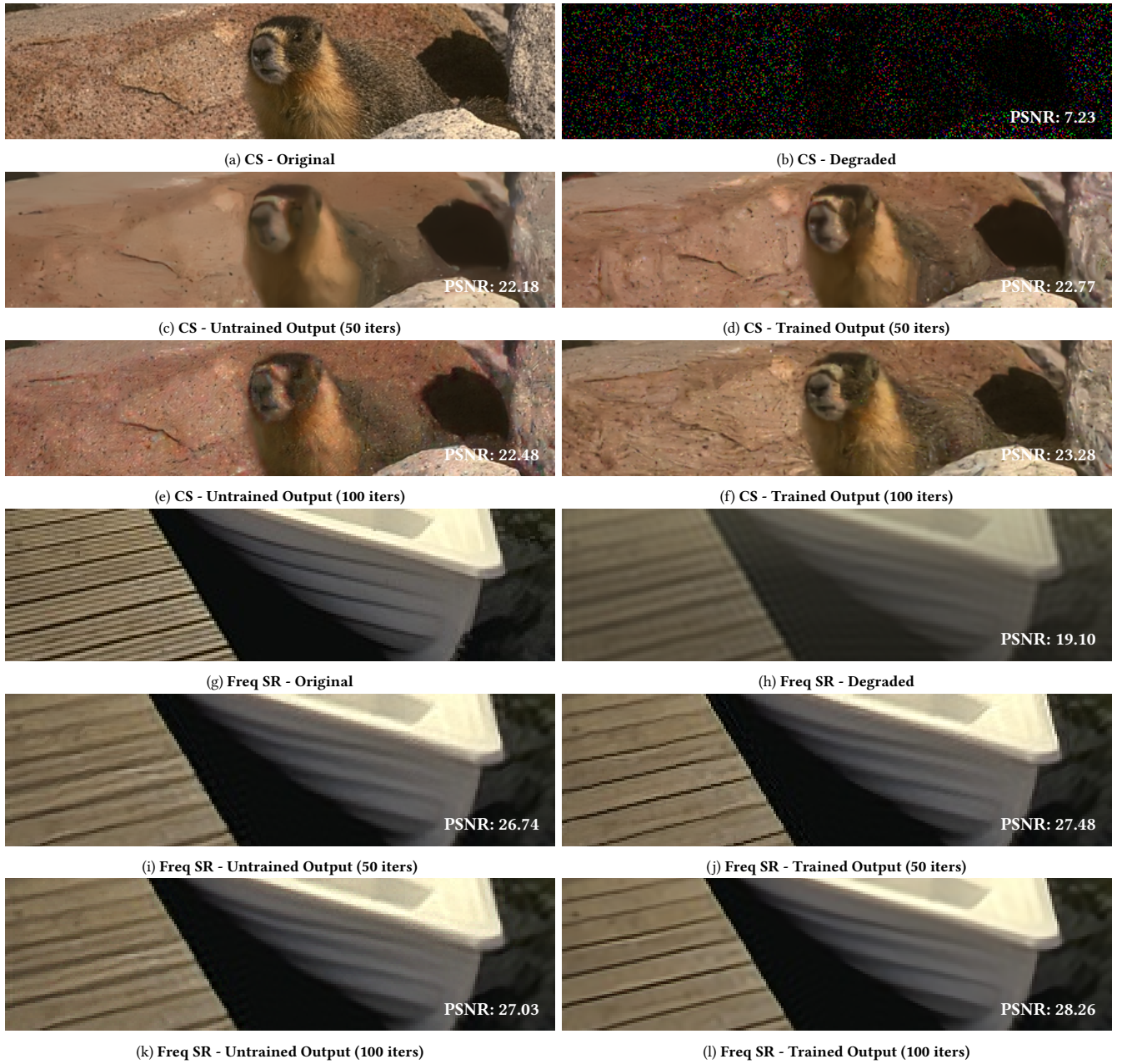


Figure 3: Sample results for two tasks: compressed sensing (top three rows) and frequency super-resolution (bottom three rows). PSNR values are shown in the bottom right of each image.

All trained networks share the same DnCNN backbone and differ only in the set of tasks used during fine-tuning. We define each configuration as follows:

- **BF-CNN:** The original, publicly available bias-free DnCNN model trained solely for denoising. This network is not fine-tuned further and serves as a fixed baseline.
- **3 Task:** In this configuration, we fine-tune the BF-CNN model using three iterative tasks: inpainting, super-resolution, and compressed sensing. The denoising task is excluded.
- **3 Task + D:** This configuration extends the 3 Task setup by including an additional denoising objective, where the noise standard deviation is sampled uniformly as $\sigma \sim U(0, 100)$. Unlike the other tasks, denoising is performed in a single forward pass rather than iteratively. This reduces training

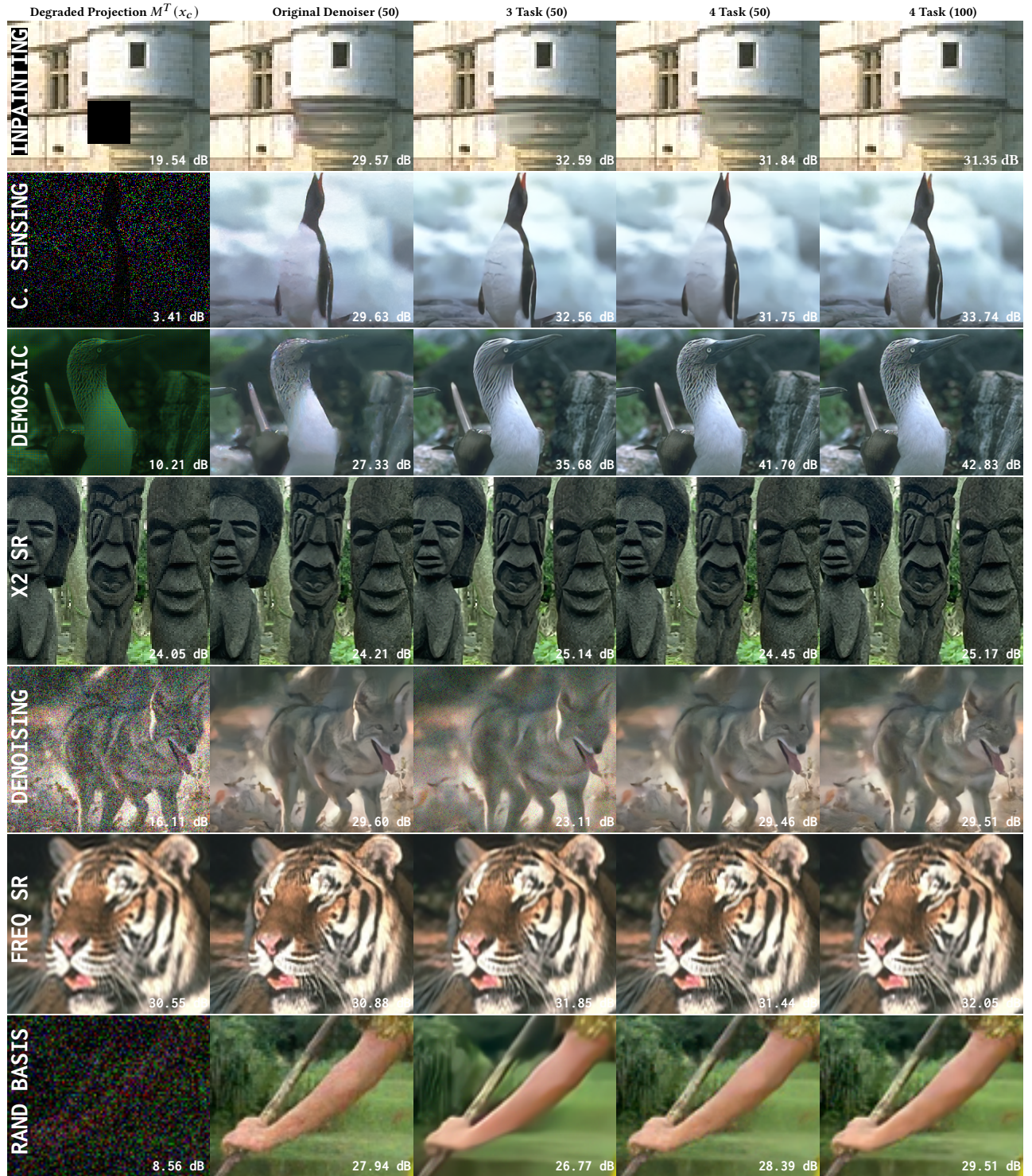


Figure 4: Sample Results of trained denoisers for inverse solving. Each column represents a different denoiser and each row represents a different task. From left to right we show the projection of the constrained measurement matrix x_c , the result of using the original BF-CNN denoiser prior, the 3 task fine-tuned prior and the 4-task, normalised loss fine-tuned denoiser. From top to bottom, the following tasks are shown: inpainting, $\times 2$ super-resolution, $\sigma = 40$ AWGN denoising, frequency super resolution, 10% random basis reconstruction.

Table 2: Table of weights used for the equalised loss scheme in training. Here, w are saved from previous losses to balance contributions from tasks.

	Inpnt.	SRx2	Sens.	$\sigma = 5$	$\sigma = 10$	$\sigma = 20$	$\sigma = 30$	$\sigma = 40$	$\sigma = 50$
$1/w$	0.014	0.035	0.048	0.011	0.017	0.026	0.033	0.040	0.046

complexity and reflects the structure of the reverse process in diffusion models.

5.2 Loss Weighting Scenarios

Some tasks produce loss values that converge to different scales due to varying task difficulties, causing tasks with smaller loss values to stop contributing to training early and underperform in testing, relative to their single-task training results. Essentially, the loss in the Multi-Task configuration amounts to a weighted average over the tasks $\mathcal{L}_{\text{total}} = \sum_{i=0}^N w_i \mathcal{L}_{\text{task}_i}$. We consider here to adjust the relative weights of each task according to different strategies:

Uniform. In this configuration, each task is assigned an equal weight of 1: $w_{\text{all}} = 1$.

Fixed. The model is biased towards the denoising tasks, with $w_{\text{denoise}} = 5$, while all other weights remain at 1.

Normalised. The loss function is optimised to balance the impact of each task on gradient computation, preventing tasks with larger loss values from disproportionately influencing the optimisation process. The weight for each task is defined as $w_i = 1/\mathcal{L}_{\text{task}_i}^{\text{prev}}$, where $\mathcal{L}_{\text{task}_i}^{\text{prev}}$ is the loss value of task i from a prior training run. For the denoising task, weights are interpolated based on the sampled noise standard deviation. The precomputed weights are summarised in Table 2.

5.3 Length of Iterations

As discussed in Section 4.4, we configure the framework to converge at a different number of iterations. In our experiments, we assess both the original BF-CNN model (with optimised scheduling parameters) and our fine-tuned model in the 50 iteration configuration and the 100 iteration configuration.

6 Results

6.1 Linear Inverse Task Performance

In Table 3 we report PSNR results (in dB) for each network across both the trained tasks (inpainting, SR- $\times 2$, compressed sensing) and the untrained tasks (frequency SR, random basis reconstruction, demosaicing). Each value represents the mean result computed over 100 test images. For fine-tuned models, the difference in performance relative to the equivalent BF-CNN baseline is shown in parentheses. Across 12 experimental runs using different random seeds, the 95% confidence intervals for PSNR remain within 0.09 dB for all evaluated tasks, with the exception of demosaicing, which exhibits higher variability (± 0.13 dB). This indicates a high degree of consistency in the results across most tasks.

The 3 Task^U model, trained with a uniform loss weighting scheme for 50 iterations, yields substantial improvements on the tasks seen

during training: inpainting improves by +4.08 dB, super-resolution by +1.66 dB, and compressed sensing by +2.09 dB. However, this model exhibits poor generalisation to the untrained tasks, most notably with a -6.90 dB drop on demosaicing compared to the baseline. As a result, it achieves the lowest overall mean improvement across all tasks.

When the denoising task is included during training (4 Task^U), generalisation improves considerably, with a mean gain of +1.12 dB over the baseline. This inclusion also helps close the gap in demosaicing performance relative to the original denoiser.

Both the original and fine-tuned networks show improved performance when evaluated at 100 iterations. The best overall results are obtained by the 4 Task^N model, which achieves a mean PSNR of 32.53 dB—representing a +1.34 dB improvement over the baseline BF-CNN evaluated at the same iteration count.

6.2 Denoising Performance

In Table 4, we report one-shot denoising results for all iteratively trained models across a range of noise levels. As expected, the original BF-CNN model, trained exclusively for denoising, achieves the highest average PSNR (32.47 dB). In contrast, the 3 Task^U model, which excludes denoising during training, performs the worst, with an average PSNR drop of 4.65 dB relative to the baseline.

Introducing the denoising task into training substantially improves results. The 4 Task^U model recovers much of the lost performance, achieving an average within 0.93 dB of the original denoiser. Applying fixed loss weighting (4 Task^F), which emphasises denoising, further narrows the gap to just 0.23 dB. Notably, the 4 Task^N model, trained with normalised loss weighting, performs nearly identically—just 0.22 dB below the baseline—while maintaining the strongest overall performance on the inverse problems. This indicates that normalised weighting provides a favourable trade-off between task-specific accuracy and broader generalisation.

Finally, the 100-iteration version of the same model (4 Task^N) achieves slightly lower denoising performance (32.15 dB), suggesting a small degradation which may result from prolonged exposure to high noise levels during iterative training, or the distribution shift introduced by additional solver iterations.

6.3 Visual Assessment

Figure 3 presents reconstructed samples from the test dataset for two tasks: compressive sensing (10%) and frequency super-resolution. For each task, we show the original image, its degraded counterpart, the 50-iteration reconstruction using the original model (BF-CNN), and the 100-iteration output using the fine-tuned model (4 Task^N).

In the compressive sensing examples, notable differences are observed in texture synthesis. Across all samples, the iterative solver generates distinct textures in the rocky background. The trained models consistently recover sharper high-frequency details—especially around the rodent’s face and the surrounding terrain. For instance, the 100-iteration trained model is able to reconstruct fine hair on the rodent’s neck that is entirely absent from the BF-CNN output.

Similar improvements are observed in the frequency super-resolution samples. The wooden pier in the original image contains strong diagonal structures which are better preserved by the trained models.

Table 3: PSNR Results (dB) for solving linear inverse problems using various denoiser training strategies. BF-CNN denotes the model weights used by Kadkhodaie, 3 Task is trained on three iterative tasks: inpainting, $\times 2$ super-resolution, and compressed sensing. 4 Task adds a fourth, non-iterative denoising task ($\sigma \sim U(0, 100)$). Superscripts indicate the loss weighting scheme: ^U = uniform, ^F = fixed, ^N = normalised. Differences (in parentheses) are relative to BF-CNN at the same iteration setting. With the exception of demosaicing, all values lie within 0.09 dB 95% confidence intervals across repeated runs.

		Degraded	BF-CNN	3 Task ^U	4 Task ^U	4 Task ^F	4 Task ^N	BF-CNN	4 Task ^N
	Iterations	-	50	50	50	50	50	100	100
<i>trained</i>	Inpainting	23.27	33.67	37.75 (+4.08)	36.89 (+3.22)	36.61 (+2.94)	37.36 (+3.69)	36.16	37.41 (+1.25)
	SR- $\times 2$	27.32	28.06	29.72 (+1.66)	29.22 (+1.16)	28.61 (+0.55)	27.36 (-0.70)	28.78	29.78 (+1.00)
	Sensing	7.33	24.79	26.88 (+2.09)	26.28 (+1.49)	25.54 (+0.75)	26.27 (+1.48)	25.22	27.09 (+1.87)
<i>untrained</i>	Freq. SR	27.65	29.92	30.95 (+1.03)	30.59 (+0.67)	30.24 (+0.32)	29.38 (-0.54)	30.30	31.23 (+0.93)
	Rand. Basis	7.53	29.26	27.66 (-1.60)	30.46 (+1.20)	29.36 (+0.10)	30.50 (+1.24)	29.10	31.45 (+2.35)
	Demosaic	8.68	38.74	31.84 (-6.90)	37.70 (-1.04)	36.36 (-2.38)	37.47 (-1.27)	37.59	38.22 (+0.63)
	Mean	16.96	30.74	30.80 (+0.06)	31.86 (+1.12)	31.12 (+0.38)	31.39 (+0.65)	31.19	32.53 (+1.34)

Table 4: PSNR (dB) Denoising results across varying noise levels σ .

Model	Input	BF-CNN	3-Task ^U	4-Task ^U	4-Task ^F	4-Task ^N	4-Task ^N	
Iterations	50	50	50	50	50	50	100	
<i>Noise STD.</i>	$\sigma = 5$	34.17	39.94	37.50 (-2.44)	39.19 (-0.75)	39.20 (-0.74)	39.60 (-0.34)	39.25 (-0.35)
	$\sigma = 10$	28.15	35.91	32.95 (-2.96)	35.56 (-0.35)	35.71 (-0.20)	35.79 (-0.12)	35.35 (-0.44)
	$\sigma = 20$	22.13	32.17	27.92 (-4.25)	31.59 (-0.58)	32.09 (-0.08)	32.01 (-0.16)	31.92 (-0.25)
	$\sigma = 30$	18.61	30.16	24.84 (-5.32)	29.29 (-0.87)	30.07 (-0.09)	29.97 (-0.19)	29.99 (-0.31)
	$\sigma = 40$	16.11	28.81	22.67 (-6.14)	27.56 (-1.25)	28.70 (-0.11)	28.58 (-0.23)	28.67 (-0.13)
	$\sigma = 50$	14.17	27.82	21.01 (-6.81)	26.04 (-1.78)	27.68 (-0.14)	27.52 (-0.30)	27.68 (-0.14)
Mean	22.22	32.47	27.82 (-4.65)	31.54 (-0.93)	32.24 (-0.23)	32.25 (-0.22)	32.15 (-0.32)	

These structures appear blurred or softened in the BF-CNN output but are much more clearly defined after fine-tuning. Additionally, while both trained models improve edge fidelity, the 100-iteration variant produces a smoother result and reduces the staircasing artefacts that remain visible in the 50-iteration version.

Additional samples are provided in Figure 4 comparing the baseline model, 3 Task^U (50), 4 Task^N (50) and 4 Task^N (100).

6.4 Summary of Findings

Training a denoiser within the linear inverse solving framework proves effective, leading to consistent improvements across multiple restoration tasks. However, when denoising is excluded from the training process, denoising performance suffers significantly, highlighting its importance for generalisation. This is due to the large variations in loss magnitudes introduced by the denoising task during training, which complicate optimisation. Emphasising the denoising loss through a fixed weighting scheme improves denoising performance, however, the normalised loss scheme provides a more balanced result between denoising and linear inverse task accuracy. Additionally, extending the number of iterations during inference further enhances visual quality, producing smoother and more detailed reconstructions.

7 Conclusions

This work has shown that the denoiser responsible for generating the image prior gradient in an iterative linear inverse solving framework can be effectively fine-tuned to improve performance across multiple inverse problem tasks. By training a single light-weight denoising network jointly on a range of inverse problems, we achieve improved generalisation while reducing the number of required solver iterations compared to the original baseline. Our quantitative results demonstrate a mean improvement of 1.34 dB across all evaluated tasks, and qualitative assessments further reveal enhanced preservation of high-frequency detail and smoother reconstructions. These findings highlight the potential of jointly training denoisers within iterative frameworks, and open the door to future work involving larger, more expressive denoising networks.

References

- Eirikur Agustsson and Radu Timofte. 2017. Ntire 2017 challenge on single image super-resolution: Dataset and study. In *Proceedings of the IEEE conference on computer vision and pattern recognition workshops*. 126–135.
- Clement Bled and Francois Pitie. 2022. Assessing advances in real noise image denoisers. In *Proceedings of the 19th ACM SIGGRAPH European Conference on Visual Media Production*. 1–9.
- Stephen Boyd, Neal Parikh, Eric Chu, Borja Peleato, Jonathan Eckstein, et al. 2011. Distributed optimization and statistical learning via the alternating direction method of multipliers. *Foundations and Trends® in Machine learning* 3, 1 (2011), 1–122.
- Alon Brifman, Yaniv Romano, and Michael Elad. 2016. Turning a denoiser into a super-resolver using plug and play priors. In *2016 IEEE International Conference on Image Processing (ICIP)*. IEEE, 1404–1408.
- Giannis Daras, Hyungjin Chung, Chieh-Hsin Lai, Yuki Mitsufuji, Jong Chul Ye, Peyman Milanfar, Alexandros G Dimakis, and Mauricio Delbracio. 2024. A survey on diffusion models for inverse problems. *arXiv preprint arXiv:2410.00083* (2024).
- Prafulla Dhariwal and Alexander Nichol. 2021. Diffusion models beat gans on image synthesis. *Advances in neural information processing systems* 34 (2021), 8780–8794.
- David L Donoho. 2006. Compressed sensing. *IEEE Transactions on information theory* 52, 4 (2006), 1289–1306.
- Bradley Efron. 2011. Tweedie's formula and selection bias. *J. Amer. Statist. Assoc.* 106, 496 (2011), 1602–1614.
- Shi Guo, Zifei Yan, Kai Zhang, Wangmeng Zuo, and Lei Zhang. 2019. Toward convolutional blind denoising of real photographs. In *Proceedings of the IEEE/CVF conference on computer vision and pattern recognition*. 1712–1722.
- Zahra Kadkhodaie and Eero Simoncelli. 2021. Stochastic solutions for linear inverse problems using the prior implicit in a denoiser. *Advances in Neural Information Processing Systems* 34 (2021), 13242–13254.
- Zahra Kadkhodaie and Eero P Simoncelli. 2020. Solving linear inverse problems using the prior implicit in a denoiser. *arXiv preprint arXiv:2007.13640* (2020).
- Yawei Li, Kai Zhang, Jingyun Liang, Jiezhong Cao, Ce Liu, Rui Gong, Yulun Zhang, Hao Tang, Yun Liu, Denis Demandolx, et al. 2023. Lsdri: A large scale dataset for image restoration. In *Proceedings of the IEEE/CVF Conference on Computer Vision and Pattern Recognition*. 1775–1787.
- Jingyun Liang, Jiezhong Cao, Yuchen Fan, Kai Zhang, Rakesh Ranjan, Yawei Li, Radu Timofte, and Luc Van Gool. 2024. VRT: A Video Restoration Transformer. *Trans. Img. Proc.* 33 (Jan. 2024), 2171–2182. doi:10.1109/TIP.2024.3372454
- Ze Liu, Yutong Lin, Yue Cao, Han Hu, Yixuan Wei, Zheng Zhang, Stephen Lin, and Baining Guo. 2021. Swin transformer: Hierarchical vision transformer using shifted windows. In *Proceedings of the IEEE/CVF International Conference on Computer Vision*. 10012–10022.
- Xiaobin Lu, Xiaobin Hu, Jun Luo, Ben Zhu, Yaping Ruan, and Wenqi Ren. 2024. 3d priors-guided diffusion for blind face restoration. In *Proceedings of the 32nd ACM International Conference on Multimedia*. 1829–1838.
- David Martin, Charless Fowlkes, Doron Tal, and Jitendra Malik. 2001. A database of human segmented natural images and its application to evaluating segmentation algorithms and measuring ecological statistics. In *Proceedings eighth IEEE international conference on computer vision. ICCV 2001*, Vol. 2. IEEE, 416–423.
- Koichi Miyasawa et al. 1961. An empirical Bayes estimator of the mean of a normal population. *Bull. Inst. Internat. Statist* 38, 181–188 (1961), 1–2.
- Sreyas Mohan, Zahra Kadkhodaie, Eero P Simoncelli, and Carlos Fernandez-Granda. 2019. Robust and interpretable blind image denoising via bias-free convolutional neural networks. *arXiv preprint arXiv:1906.05478* (2019).
- Alexander Quinn Nichol and Prafulla Dhariwal. 2021. Improved denoising diffusion probabilistic models. In *International conference on machine learning*. PMLR, 8162–8171.
- Peng Qiao, Yong Dou, Wensen Feng, Rongchun Li, and Yunjin Chen. 2017. Learning non-local image diffusion for image denoising. In *Proceedings of the 25th ACM international conference on Multimedia*. 1847–1855.
- Jiahuan Ren, Zhao Zhang, Richang Hong, Mingliang Xu, Haijun Zhang, Mingbo Zhao, and Meng Wang. 2022. Robust low-rank convolution network for image denoising. In *Proceedings of the 30th ACM International Conference on Multimedia*. 6211–6219.
- Herbert E Robbins. 1992. An empirical Bayes approach to statistics. In *Breakthroughs in Statistics: Foundations and basic theory*. Springer, 388–394.
- Yaniv Romano, Michael Elad, and Peyman Milanfar. 2017. The little engine that could: Regularization by denoising (RED). *SIAM Journal on Imaging Sciences* 10, 4 (2017), 1804–1844.
- Jascha Sohl-Dickstein, Eric Weiss, Niru Maheswaranathan, and Surya Ganguli. 2015. Deep unsupervised learning using nonequilibrium thermodynamics. In *International conference on machine learning*. PMLR, 2256–2265.
- Jiaming Song, Chenlin Meng, and Stefano Ermon. 2020. Denoising diffusion implicit models. *arXiv preprint arXiv:2010.02502* (2020).
- Jingfan Tan, Hyunhee Park, Ying Zhang, Tao Wang, Kaihao Zhang, Xiangyu Kong, Pengwen Dai, Zikun Liu, and Wenhan Luo. 2024. Blind face video restoration with temporal consistent generative prior and degradation-aware prompt. In *Proceedings of the 32nd ACM International Conference on Multimedia*. 1417–1426.
- Matias Tassano, Julie Delon, and Thomas Veit. 2019. Dvdnet: A fast network for deep video denoising. In *2019 IEEE International Conference on Image Processing (ICIP)*. IEEE, 1805–1809.
- Matias Tassano, Julie Delon, and Thomas Veit. 2020. Fastdvdnet: Towards real-time deep video denoising without flow estimation. In *Proceedings of the IEEE/CVF conference on computer vision and pattern recognition*. 1354–1363.
- Singanallur V Venkatakrishnan, Charles A Bouman, and Brendt Wohlberg. 2013. Plug-and-play priors for model based reconstruction. In *2013 IEEE global conference on signal and information processing*. IEEE, 945–948.
- Hongjie Wu, Linchao He, Mingqin Zhang, Dongdong Chen, Kunming Luo, Mengting Luo, Ji-Zhe Zhou, Hu Chen, and Jiancheng Lv. 2024a. Diffusion Posterior Proximal Sampling for Image Restoration. In *Proceedings of the 32nd ACM International Conference on Multimedia*. 214–223.
- Yuhui Wu, Guoqing Wang, Zhiwen Wang, Yang Yang, Tianyu Li, Malu Zhang, Chongyi Li, and Heng Tao Shen. 2024b. JoReS-Diff: Joint Retinex and Semantic Priors in Diffusion Model for Low-light Image Enhancement. In *Proceedings of the 32nd ACM International Conference on Multimedia*. 1810–1818.
- Chenggang Yan, Zhisheng Li, Yongbing Zhang, Yutao Liu, Xiangyang Ji, and Yongdong Zhang. 2020. Depth image denoising using nuclear norm and learning graph model. *ACM Transactions on Multimedia Computing, Communications, and Applications (TOMM)* 16, 4 (2020), 1–17.
- Huanjing Yue, Cong Cao, Lei Liao, and Jingyu Yang. 2023. RViDeformer: Efficient Raw Video Denoising Transformer with a Larger Benchmark Dataset. *arXiv e-prints* (2023), arXiv–2305.
- Kai Zhang, Yawei Li, Wangmeng Zuo, Lei Zhang, Luc Van Gool, and Radu Timofte. 2021. Plug-and-play image restoration with deep denoiser prior. *IEEE Transactions on Pattern Analysis and Machine Intelligence* 44, 10 (2021), 6360–6376.
- Kai Zhang, Wangmeng Zuo, Yunjin Chen, Deyu Meng, and Lei Zhang. 2017a. Beyond a gaussian denoiser: Residual learning of deep cnn for image denoising. *IEEE transactions on image processing* 26, 7 (2017), 3142–3155.
- Kai Zhang, Wangmeng Zuo, Shuhang Gu, and Lei Zhang. 2017b. Learning Deep CNN Denoiser Prior for Image Restoration. In *Proceedings of the IEEE Conference on Computer Vision and Pattern Recognition (CVPR)*. 3929–3938. https://openaccess.thecvf.com/content_cvpr_2017/html/Zhang_Learning_Deep_CNN_CVPR_2017_paper.html